# The reduction and oxidation of cationic carbonyl complexes of manganese with phosphoniodithioformate: X-ray crystal structure of $[Mn(CO)_4(S_2CPCy_3)]ClO_4$

Gabino A. Carriedo [a,*], Julio A. Pérez-Martínez [a], Daniel Miguel [a], Víctor Riera [a], Santiago García-Granda [b], Enrique Pérez-Carreño [b]

[a] Instituto Universitario de Química Organometálica "Enrique Moles", Unidad Asociada al CSIC, Facultad de Química, Universidad de Oviedo, 33071 Oviedo, Spain
[b] Departamento de Química Física y Analítica, Facultad de Química, Universidad de Oviedo, 33071 Oviedo, Spain

## Abstract

Manganese carbonyl complexes of the types $[Mn(CO)_4(S_2CPCy_3)]ClO_4$ (1), $fac$-$[Mn(CO)_3L(S_2CPCy_3)]ClO_4$(L = P(OMe)_3 (2a), PCy_3 (2b), or PEt_3 (2c)), and $cis,trans$-$[Mn(CO)_2L_2(S_2CPR_3)]ClO_4$(R = Cy, L = P(OMe)_3 (3a), R=Cy, L = PEt_3 (3b), R = Et, L = PEt_3 (3c)) have been prepared, and the crystal structure of compound (1) has been determined by X-ray diffraction. Their redox behaviour have been studied by cyclic voltammetry and controlled potential electrolysis, showing that they undergo one-electron reduction and one-electron oxidation at potentials that depend mainly on the number of carbonyls. The results have been explained on the basis on an MO study at an EH level carried out on the model complexes $[Mn(CO)_4(S_2CPH_3)]^+$ (1b), $fac$-$[Mn(CO)_3PH_3(S_2CPH_3)]^+$ (2d), $cis,trans$-$[Mn(CO)_2(PH_3)_2(S_2CPH_3)]^+$ (3d), $mer$-$[Mn(CO)_3PH_3(S_2CPH_3)]^+$ (4), $trans,cis$-$[Mn(CO)_2(PH_3)_2(S_2CPH_3)]^+$ (5), and $cis,cis$-$[Mn(CO)_2(PH_3)_2(S_2CPH_3)]^+$(6).

Keywords: Manganese; Phosphoniodithioformate complexes; X-ray crystal structure; Electrochemistry; Carbonyls; Molecular orbital calculations

## 1. Introduction

Previously we have reported the syntheses of various cationic carbonyl complexes of manganese with $S_2CPR_3$, of the types $[Mn(CO)_4(S_2CPCy_3)]ClO_4$ [1], $fac$-$[Mn(CO)_3L(S_2CPCy_3)]ClO_4$ [1], and $cis,trans$-$[Mn(CO)_2L_2(S_2CPR_3)]ClO_4$ [2,3].

No electrochemical studies have been carried out on complexes of these types, and we have now prepared new derivatives and studied their reduction and oxidation.

Here we describe the results and an explanation based on a molecular orbital study at the extended Hückel level carried out on the model complexes having $PH_3$

## 2. Results and discussion

For this study, the complexes $[Mn(CO)_4(S_2CPCy_3)]$-$ClO_4$ (1) [1], $fac$-$[Mn(CO)_3L(S_2CPCy_3)]ClO_4$ (L = P(OMe)_3 (2a) [1], PCy_3 (2b) [1], or PEt_3 (2c)), and $cis,trans$-$[Mn(CO)_2L_2(S_2CPR_3)]ClO_4$ (R = Cy, L = P(OMe)_3 (3a) [3], R = Cy, L = PEt_3 (3b), R = Et, L = PEt_3 (3c) [2]) (Fig. 1) were prepared following the methods described previously. Data for the new complexes 2c and 3b, are given in Section 3.

In the case of the tetracarbonyl $[Mn(CO)_4(S_2CPCy_3)]ClO_4$ (1), the structure was determined by X-ray diffraction. Crystal and refinement details are collected in Table 1, atomic parameters in Table 2, and bond lengths and angles in Table 3. A perspective view of the structure is depicted in Fig. 2. The most interesting feature is the high symmetry of the cation. It is on a crystallographic mirror plane through the atoms Mn, C(1), P(1), the axial carbonyls C(2)–O(2) and C(3)–O(3) and the atoms C(11) and C(14) of one cyclohexyl
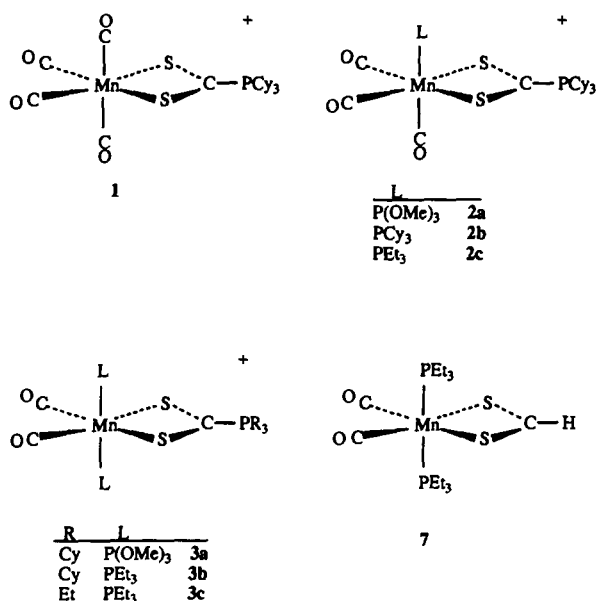
* Corresponding author.

Fig. 1. Structural formulae of the octahedral manganese carbonyls complexes with S₂CPR₃.

ring. The distances Mn–S, S–C, C–P, and Mn–C(carbonyl) are similar, within experimental error, to those found in the structures of other cationic complexes containing phosphoniodithioformate, such as fac-[Mn(CO)₃(S₂CPCy₃)₂]ClO₄ [1], and cis,trans-[Mn-

Table 1
Crystallographic data for [Mn(CO)₄(S₂CPCy₃)]ClO₄ (1)

| Formula | C₂₃H₃₃ClMnO₈PS₂ |
|---|---|
| Formula weight | 622.99 |
| Crystal system, space group | orthorhombic, Cmca |
| a (Å) | 11.088(3) |
| b (Å) | 19.986(3) |
| c (Å) | 26.356(4) |
| V (Å³) | 5840(2) |
| Z | 8 |
| T (K) | 293 |
| ρcalc (g cm⁻³) | 1.41 |
| F(000) | 2592 |
| λ (Mo Kα) (Å) | 0.71073 |
| μ (cm⁻¹) | 7.58 |
| Crystal size (mm) colour | 0.30×0.14×0.10; red |
| Method of collection | ω/2θ scan |
| Scan range (deg) | 1 ≤ θ ≤ 25, |
| Collection limits | 0 ≤ h ≤ 13, 0 ≤ k ≤ 13, 0 ≤ l ≤ 31 |
| No. of reflections collected | 2863 |
| No. of reflections observed | 1038 [I ≥ 3σ(I)] |
| Absorption correction | psi-scan |
| factors: max, min | 0.999, 0.969 |
| No. of parameters | 188 |
| Data to parameters ratio | 5.52 |
| Weighting scheme | w = [σ²(F)+ gF²]⁻¹ |
| g | 0.0006 |
| Residuals [a] R, Rw | 0.049, 0.050 |

[a] $R = \Sigma(||F_o| - |F_c||)/\Sigma|F_o|$; $Rw = \{\Sigma[w(|F_o| - |F_c|)^2]/\Sigma w|F_o|^2\}^{1/2}$.

Table 2
Atomic coordinates and equivalent [a] isotropic displacement coefficients (Å²) for [Mn(CO)₄(S₂CPCy₃)]ClO₄ (1)

| Atom | x | y | z | $U_{eq}$ (×100) |
|---|---|---|---|---|
| Mn | 0.50000 | 0.21233(9) | 0.73564(6) | 4.07(6) |
| C(2) | 0.50000 | 0.1472(7) | 0.7829(6) | 6.3(6) |
| O(2) | 0.50000 | 0.1060(6) | 0.8135(4) | 10.4(5) |
| C(3) | 0.50000 | 0.2776(7) | 0.6864(5) | 6.7(6) |
| O(3) | 0.50000 | 0.3192(5) | 0.6570(4) | 11.2(6) |
| C(4) | 0.3779(9) | 0.1685(4) | 0.7032(3) | 5.3(3) |
| O(4) | 0.2977(6) | 0.1410(4) | 0.6860(3) | 8.8(3) |
| S(1) | 0.3739(2) | 0.2769(1) | 0.78880(8) | 4.93(8) |
| C(1) | 0.50000 | 0.3036(5) | 0.8176(4) | 3.4(4) |
| P | 0.50000 | 0.3506(2) | 0.8757(1) | 3.6(1) |
| C(11) | 0.50000 | 0.2896(6) | 0.9270(4) | 4.0(4) |
| C(12) | 0.3847(7) | 0.2456(4) | 0.9270(3) | 5.2(3) |
| C(13) | 0.3867(9) | 0.1980(4) | 0.9726(4) | 6.8(4) |
| C(14) | 0.50000 | 0.1544(7) | 0.9721(6) | 6.8(6) |
| C(21) | 0.3596(7) | 0.3973(4) | 0.8767(3) | 4.2(3) |
| C(22) | 0.3333(9) | 0.4305(5) | 0.9277(3) | 6.6(4) |
| C(23) | 0.204(1) | 0.4581(5) | 0.9259(4) | 8.9(5) |
| C(24) | 0.184(1) | 0.5072(5) | 0.8826(4) | 7.9(5) |
| C(25) | 0.2152(9) | 0.4743(5) | 0.8332(4) | 7.4(4) |
| C(26) | 0.3436(8) | 0.4476(4) | 0.8332(3) | 5.5(3) |
| CL | 0.50000 | 0.1357(2) | 0.5752(1) | 6.8(2) |
| O(11) | 0.50000 | 0.0896(5) | 0.6156(3) | 7.6(4) |
| O(12) | 0.50000 | 0.1955(5) | 0.5919(5) | 31.(2) |
| O(13) | 0.407(1) | 0.1254(8) | 0.5432(4) | 24.4(8) |

[a] $U_{eq}$ defined as one third of the trace of the orthogonalized $U_{ij}$ tensor.

(CO)₂(PEt₃)₂(S₂CPEt₃)]ClO₄ (3c) [2]. Therefore, it seems that, as in all other octahedral manganese carbonyls, the substitution of CO by PR₃ does not alter significantly the bond distances, even though the more basic phosphines should increase the electron richness of the Mn atom, affecting both the Mn–CO and the Mn–S bonds. As in the other structures with S₂CPR₃ mentioned above, the maximum deviation from the octahedral geometry in the cation of 1 comes from the small bite angle of the S₂CPCy₃ (S(1)–Mn–S(1′) is 72.6(1)°). This permits a greater angle between the carbonyl groups on the opposite side of the 'equatorial' plane (C(4)–Mn–C(4′)=95.7(4)°).

We measured the cyclic voltammograms of these complexes in dichloromethane solution in the range −1.6 to +1.8 V.

The cyclic voltammogram of the tetracarbonyl 1 exhibits a diffusion-controlled one-electron reduction wave with a $E_{1/2}$ near −0.5 V (see Table 4). It showed some reversibility only at high scan rates (see Figs. 3(a) and 3(b)). The voltammogram also shows a second irreversible reduction wave (II in Fig. 3) at more negative potentials that was less intense at higher scan rates. This might indicate that the neutral radical formed in the reduction decomposes slowly to another redox-active product, but because of the lack of stability of the reduced species it could not be confirmed. The lack of a distinct oxidation wave in the cyclic voltammogram of

Table 3
Bond lengths (Å) and angles (deg) for $[Mn(CO)_4(S_2CPCy_3)]ClO_4$ (1)

| | | | |
|---|---|---|---|
| Mn–C(2) | 1.80(2) | Mn–C(3) | 1.84(1) |
| Mn–C(4) | 1.825(9) | Mn–S(1) | 2.363(3) |
| C(2)–O(2) | 1.15(1) | C(3)–O(3) | 1.13(1) |
| C(4)–O(4) | 1.139(9) | S(1)–C(1) | 1.679(6) |
| C(1)–P | 1.80(1) | P–C(11) | 1.82(1) |
| P–C(21) | 1.815(7) | C(11)–C(12) | 1.55(1) |
| C(12)–C(13) | 1.53(1) | C(13)–C(14) | 1.53(1) |
| C(21)–C(22) | 1.53(1) | C(21)–C(26) | 1.54(1) |
| C(22)–C(23) | 1.54(1) | C(23)–C(24) | 1.52(1) |
| C(24)–C(25) | 1.50(1) | C(25)–C(26) | 1.52(1) |
| CL–O(11) | 1.408(8) | CL–O(12) | 1.27(1) |
| CL–O(13) | 1.350(9) | | |
| | | | |
| C(3)–Mn–C(2) | 178.9(6) | C(4)–Mn–C(2) | 88.7(4) |
| C(4)–Mn–C(3) | 90.6(4) | S(1)–Mn–C(2) | 89.1(4) |
| S(1)–Mn–C(3) | 91.8(3) | S(1)–Mn–C(4) | 95.8(3) |
| S(1')–Mn–S(1) | 72.6(1) | C(4')–Mn–S(1) | 168.2(3) |
| C(4')–Mn–C(4) | 95.7(4) | O(2)–C(2)–Mn | 179.(1) |
| O(3)–C(3)–Mn | 178.(1) | O(4)–C(4)–Mn | 175.3(9) |
| C(1)–S(1)–Mn | 87.1(3) | S(1')–C(1)–S(1) | 112.8(1) |
| P–C(1)–S(1) | 123.5(1) | C(11)–P–C(1) | 106.4(5) |
| C(21)–P–C(1) | 106.3(3) | C(21)–P–C(11) | 109.5(3) |
| C(21')–P–C(21) | 118.2(3) | C(12)–C(11)–P | 112.3(6) |
| C(13)–C(12)–C(11) | 109.9(8) | C(12')–C(11)–C(12) | 110.9(4) |
| C(14)–C(13)–C(12) | 111.0(9) | C(13')–C(14)–C(13) | 110.6(5) |
| C(22)–C(21)–P | 113.5(6) | C(26)–C(21)–P | 115.1(6) |
| C(26)–C(21)–C(22) | 110.5(6) | C(23)–C(22)–C(21) | 107.8(8) |
| C(24)–C(23)–C(22) | 112.9(9) | C(25)–C(24)–C(23) | 109.6(8) |
| C(26)–C(25)–C(24) | 111.7(9) | C(25)–C(26)–C(21) | 109.7(8) |
| O(12)–CL–O(11) | 110.8(7) | O(13)–CL–O(11) | 111.9(6) |
| O(13)–CL–O(12) | 111.0(8) | O(13')–CL–O(13) | 99.9(6) |

1 indicated that the oxidation potential of this compound must be higher than 1.8 V.

The cyclic voltammograms of the complexes 2 and 3 show two diffusion-controlled waves ($i/\sqrt{c}$ = constant) (see Table 4) that were chemically irreversible (Fig. 4(a)–4(c)). The first wave, at negative potentials, corresponds to the one-electron reduction of the cations, to produce the corresponding neutral radicals, and the second wave, at positive potentials, corresponds to their oxidation to the corresponding dipositive cations.

In the case of the fac-tricarbonyl 2, the oxidation wave was fully irreversible, and the voltammograms showed a product reduction peak (MER in Fig. 4(a)) that probably corresponds to the mer-isomers, although again this could not be confirmed chemically.

In the cases of the dicarbonyls (3) the peak separations $\Delta E_p$ of the oxidation wave were significantly larger than those of the reduction wave, and for L = $P(OMe)_3$ (3a) a reduction peak of a product of the oxidation was also observed near 0.8 V (PR in Fig. 4(c)) with an intensity that increased with the scan rate. Although the results of the chemical oxidations did not

Table 4
Electrode potentials for the compounds [a]

OC–Mn with L$_1$, L$_2$, and C–L$_p$, S bridges [+]
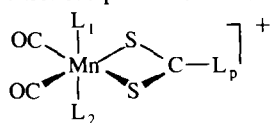
| Compound | L$_p$ | L$_1$ | L$_2$ | $E^{red}_{1/2}$ | $(i_a/i_c)$ [b] | $E^{ox}_{1/2}$ | $(i_c/i_a)$ [b] |
|---|---|---|---|---|---|---|---|
| 1 | PCy$_3$ | CO | CO | −0.55 [c,d] | (0.83) | > 1.8 [e] | irreversible |
| 2a | PCy$_3$ | P(OMe)$_3$ | CO | −0.80 | | ≈ 1.5 [e] | irreversible |
| 2b | PCy$_3$ | PCy$_3$ | CO | −0.90 | | ≈ 1.5 [e] | irreversible |
| 2c | PCy$_3$ | PEt$_3$ | CO | −0.83 | (0.93) | 1.51 [e] | irreversible |
| 3a | PCy$_3$ | P(OMe)$_3$ | P(OMe)$_3$ | −1.05 | (0.85) | 1.10 | (0.50) |
| 3b | PCy$_3$ | PEt$_3$ | PEt$_3$ | −1.14 | (0.80) | 0.91 | (0.88) |
| 3c | PEt$_3$ | PEt$_3$ | PEt$_3$ | −1.10 [f] | (0.93) | 0.86 [g] | (1.0) |
| 7 | H | PEt$_3$ | PEt$_3$ | | | 0.48 | (1.0) |

[a] Measured in $CH_2Cl_2$ solutions vs. SCE using $[N^nBu_4]PF_6$ as base-electrolyte, at 50 mV s$^{-1}$. [b] Measured at 300 mV s$^{-1}$. [c] A second reduction peak appears at −0.83 V (0.7 in THF). [d] In THF at −0.39 V. [e] The value quoted corresponds to the oxidation peak of the irreversible wave. [f] In THF at −0.97 V. [g] In THF at −0.90 V.
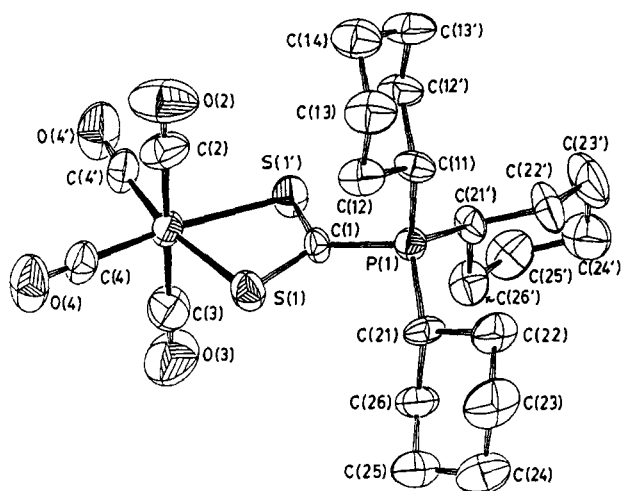
Fig. 2. Perspective view (EUCLID package) [10] of the cation [Mn(CO)₄(μ-S₂CPCy₃)]⁺ in 1, showing the atom numbering. Primed atoms are related to the unprimed ones by a crystallographic mirror plane.



Fig. 4. Cyclic voltammogram of (a) 2c, (b) 3c and (c) 3a measured in $CH_2Cl_2$ at 50 mV s⁻¹, starting at 0 V and switching the potential at (a) −1.2 and +1.7 V, (b) +1.2 and −1.5 V and (c) −1.3 and +1.3 V.

allow a confirmation, those effects can perhaps be attributed to a better thermodynamic control of the reduction processes at the electrode, and in the case of L = P(OMe)₃ to a chemical process (isomerization or decomposition) following the oxidation step.

The electrode potentials for the reduction of the complexes (Table 4), as measured in the cyclic voltammograms, showed a significant dependence on the number of CO ligands, varying from −0.55 V for the
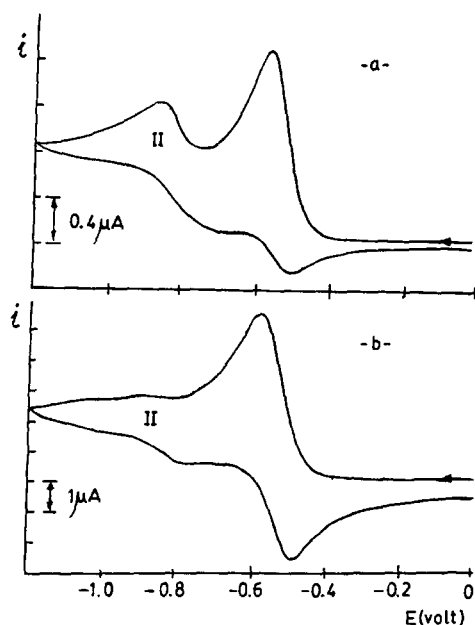
tetracarbonyl, to about −0.9 for the tricarbonyls, and about −1.1 V for the dicarbonyls, but varied little with the phosphorus ligands L in the complexes. The potentials for the reductions were slightly less negative in THF than in $CH_2Cl_2$ (Table 4).

The potentials for the oxidation were also very sensitive to the number of CO ligands, varying from more than 1.8 V for the tetracarbonyl, to about 1.5 V for the tricarbonyls, and about 1 V for the dicarbonyls. For the latter series, the potentials showed a clear correlation with the P-ligands. Changing L = PEt₃ for P(OMe)₃ increased the potential by about 0.2 V (see Table 4).

Attempts to confirm the number of electrons involved in both electron transfer processes by controlled potential electrolysis (CPE) at a platinum electrode gave poor results because of the extensive decomposition of the reduced or oxidized species. For the same reason, our attempts to obtain reduction and oxidation products by the chemical reactions led to decomposition. However, some of the results of the electrolysis and the chemical reactions gave useful information about the redox processes.



Fig. 3. Cyclic voltammogram of [Mn(CO)₄(S₂CPCy₃)]ClO₄ (1) in $CH_2Cl_2$, measured between 0 and −1.2 V, at (a) 50 mV s⁻¹ and (b) 600 mV s⁻¹.
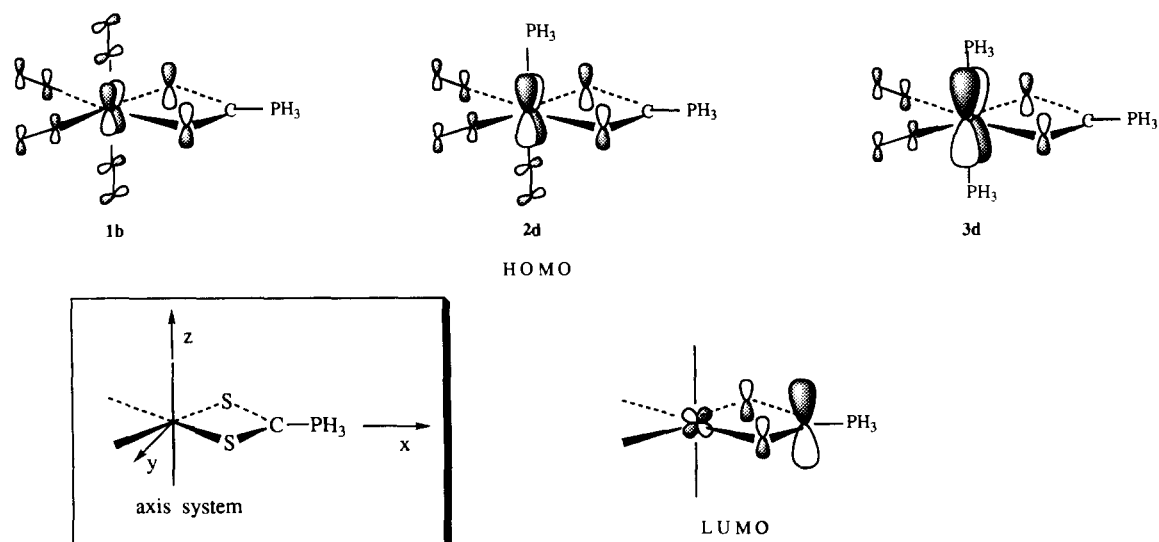
Fig. 5. A schematic drawing of the frontier orbitals of the model complexes, showing the approximate relative contributions of the composing atomic orbitals.

Thus, the reduction of the tetracarbonyl 1 with [CoCp$_2$] in toluene gave a violet solution with a signal in the ESR spectrum that, although not well-defined, could be described as a doublet. Although the instability of the radical precluded an accurate measurement of the ESR parameters, the spectrum unambiguously indicated the presence of a radical paramagnetic species with the electron coupled with the phosphorus atom, showing that it is more localized in the phosphoniodithioformate.

The reduction of the dicarbonyl 3c at a controlled potential of − 1.15 V, required more than one electron, and the ESR spectrum of the resulting solution showed no signal of any radical paramagnetic species. The reduction of the cis-trans dicarbonyl 3c with Na/Hg amalgam in THF led to a dark violet solution that was very unstable, decomposing to give the known cis,trans-[Mn(CO)$_2$(PEt$_3$)$_2$(S$_2$CH)] (7) [2] as the only identifiable product. This result suggests that the sodium

Table 5
Orbital energies (eV) and metal and S$_2$CPH$_3$ contributions to the frontier orbitals of the model compounds, as computed from the charge matrix elements [a]

| Compound | | HOMO | | | LUMO | | |
|---|---|---|---|---|---|---|---|
| | | $\varepsilon$ | Mn (%) | S$_2$CPH$_3$ (%) | $\varepsilon$ | Mn (%) | S$_2$CPH$_3$ |
| | 1b | − 12.14 | 31.45 | 43.36 | − 8.84 | 1.25 | 94.98 |
| | 2d | − 11.92 | 41.92 | 32.63 | − 8.82 | 1.40 | 94.55 |
| | 4 | − 11.82 | 70.64 | 5.79 | − 8.83 | 1.46 | 95.07 |
| | 3d | − 11.64 | 58.47 | 19.19 | − 8.78 | 2.52 | 93.29 |

[a] P = PH$_3$.

amalgam reduces the complex to the anionic species $cis,trans$-$[Mn(CO)_2(PEt_3)_2(S_2CPEt_3)]^-$ (a reduction process involving a total of two electrons a per molecule), that readily loses the $PEt_3$ group of the $S_2CPEt_3$ and is easily protonated to give the observed product.

For the oxidation of 3c at 1.1 V the number of electrons was more reasonable ($n = 1.14$). During the electrolysis a blue-violet solution of the dication was formed, and the cyclic voltammogram showed the expected reduction wave at the right potential. However, the dication was very unstable, regenerating the monocation in solution even under dinitrogen.

The experimental observations mentioned above can be explained by the results of an EHMO study carried out on the model complexes $[Mn(CO)_4(S_2CPH_3)]^+$ (1b), $fac$-$[Mn(CO)_3PH_3(S_2CPH_3)]^+$ (2d), and $cis,trans$-$[Mn(CO)_2(PH_3)_2(S_2CPH_3)]^+$ (3d) (see Section 3).

The HOMO of the cation 1b (Fig. 5) is formed from the Mn-$d_{yz}$ orbital, mixed with the corresponding combination of the $\pi^*$-antibonding orbitals of the four CO ligands, and with $\pi$-donating non-bonding orbital of the $S_2CPH_3$ fragment. It is precisely the last interaction which destabilizes the $d_{yz}$-based frontier orbital of the $Mn(CO)_4$ fragment to the extent of making it the HOMO of the complex.
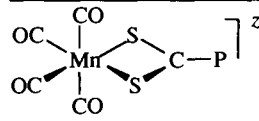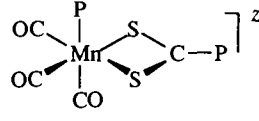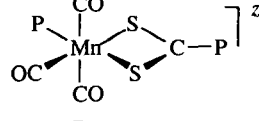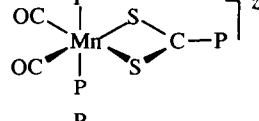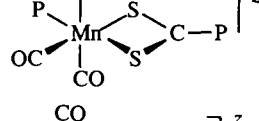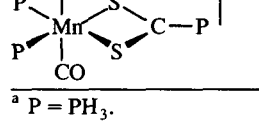
The HOMO of the tricarbonyl 2d, and the dicarbonyl 3d, are very similar to that of the tetracarbonyl (see Fig. 5), but, because of the smaller number of CO ligands, the corresponding Mn-$d_{yz}$ orbital is less stabilized d by the combination with the acceptor $\pi^*$-CO orbitals, and has a higher energy (Table 5). Also, as a consequence of the smaller number of CO ligands, the HOMO is more localized on the Mn atom, and has a lower contribution from the $\pi$-donating non-bonding orbital of the $S_2CPH_3$ fragment in the dicarbonyl than in the tricarbonyl or the tetracarbonyl (Table 5).

In contrast, the contribution of the Mn-$d_{yz}$ orbitals in the HOMO was slighty lower if the phosphorus d orbitals of the $PH_3$ ligands were included in the calculations [4].

This explains the variations of the electrode potential for the oxidation observed for the real complexes. The HOMO is more localized a the Mn atom in the case of the cis-trans dicarbonyls, consistent with the fact that in this family of complexes the electrode potentials for the oxidations change most markedly with the ligands bonded to the Mn atom.

The LUMOs of the complexes 1b, 2d and 3d (see Fig. 5) are mostly the $\pi^*$ antibonding orbital of the $S_2CPH_3$ fragment, with only a very small contribution of the Mn-$d_{xz}$ orbital. Therefore, the reduction should

Table 6
Frontier MO energies (eV) and total one-electron energies (eV) for the model complexes [a]

| Compound | | $z$ | $\varepsilon_{HOMO}$ | $\varepsilon_{LUMO}$ | $E_T$ |
|---|---|---|---|---|---|
| $OC\underset{OC}{\overset{CO}{\underset{|}{\overset{|}{Mn}}}}\langle\overset{S}{\underset{S}{}}\rangle C-P$ | 1b | 0<br>1<br>2 | $-12.14$ | $-8.84$ | $-1300.57$<br>$-1291.73$<br>$-1279.59$ |
| $OC\underset{OC}{\overset{P}{\underset{|}{\overset{|}{Mn}}}}\langle\overset{S}{\underset{S}{}}\rangle C-P$ | 2d | 0<br>1<br>2 | $-11.92$ | $-8.82$ | $-1241.12$<br>$-1232.31$<br>$-1220.38$ |
| $P\underset{OC}{\overset{CO}{\underset{|}{\overset{|}{Mn}}}}\langle\overset{S}{\underset{S}{}}\rangle C-P$ | 4 | 0<br>1<br>2 | $-11.82$ | $-8.83$ | $-1241.02$<br>$-1232.19$<br>$-1220.37$ |
| $OC\underset{OC}{\overset{P}{\underset{|}{\overset{|}{Mn}}}}\langle\overset{S}{\underset{S}{}}\rangle C-P$ | 3d | 0<br>1<br>2 | $-11.64$ | $-8.78$ | $-1181.38$<br>$-1172.60$<br>$-1160.96$ |
| $P\underset{OC}{\overset{P}{\underset{|}{\overset{|}{Mn}}}}\langle\overset{S}{\underset{S}{}}\rangle C-P$ | 6 | 0<br>1<br>2 | $-11.61$ | $-8.81$ | $-1181.29$<br>$-1172.48$<br>$-1160.87$ |
| $P\underset{P}{\overset{CO}{\underset{|}{\overset{|}{Mn}}}}\langle\overset{S}{\underset{S}{}}\rangle C-P$ | 5 | 0<br>1<br>2 | $-11.28$ | $-8.83$ | $-1181.06$<br>$-1172.23$<br>$-1160.95$ |

[a] $P = PH_3$.

be almost totally located on the $S_2CPH_3$ (affecting mainly to the C atom), which is consistent with the ESR spectrum of **1**. However, the energy of the LUMO changes very little with the number of CO ligands (see Table 5), and is almost the same for the three types of complexes, even though the experimental reduction electrode potentials show a large variation with the number of CO ligands. This shows that the LUMO energies and the electrode potentials are not correlated in a simple manner. Solvation may also be very important in the reduction, as shown by the large difference between the values obtained in $CH_2Cl_2$ and THF.

. The chemical reduction leading to the $S_2CH$ derivatives is consistent with the antibonding character of the LUMO of the $C-PR_3$ bond.

A calculation of the total energy of the other possible isomers of the tri-, and di-carbonyls $mer$-[Mn(CO)$_3$-PH$_3$(S$_2$CPH$_3$)]$^+$ (**4**), $cis,trans$-[Mn(CO)$_2$(PH$_3$)$_2$(S$_2$CP-H$_3$)]$^+$ (**5**), and $cis,cis$-[Mn(CO)$_2$(PH$_3$)$_2$(S$_2$CPH$_3$)]$^+$ (**6**) (see Table 6) showed that in no case is the oxidation or reduction processes expected to be followed by an isomerization. Thus, for the dicationic tricarbonyls the energies are about the same for both $fac$ and $mer$ isomers, which contrasts with the usual situation in manganese tricarbonyls [5–7].

## 3. Experimental section

All reactions were carried out under dry dinitrogen with standard Schlenk techniques. IR spectra were recorded with Perkin–Elmer FT 1720-X spectrometer. NMR spectra were recorded on a Bruker AC-300 instrument. Elemental analyses were performed with a Perkin Elmer 240 microanalyser. The cyclic voltammograms measured with a PAR M273 instrument. The auxiliary electrode was a platinum wire, and the working electrode was a platinum bead. The reference was a calomel electrode, separated from the solution by a fine-porosity frit and an agar–agar bridge saturated with KCl. Solutions were $0.5 \times 10^{-3}$ M in the complexes and 0.1 M in N$^n$Bu$_4$[PF$_6$] as supporting electrolyte. Under the same experimental conditions $E_{1/2}$ for the ferrocene–ferricinium couple was 0.46 V, with a peak separation of 76 mV.

### 3.1. fac-[Mn(CO)$_3$(PEt$_3$)(S$_2$CPCy$_3$)] ClO$_4$ (2c)

A mixture of $fac$-[Mn(CO)$_3$Br(S$_2$CPCy$_3$)] [1] (0.3 g, 0.521 mmol) and AgClO$_4$ (0.13 g, 0.625 mmol) in CH$_2$Cl$_2$ (25 cm$^3$) was stirred in the dark for 2 h, until IR monitoring showed the complete formation of $fac$-[Mn(CO)$_3$(OClO$_3$)(S$_2$CPCy$_3$)] ($\nu$(CO) bands at 2030 s, 1950 s, and 1935 s, cm$^{-1}$) [1]. The solids were filtered off, and to the purple solution was added PEt$_3$ (77 $\mu$l, 0.521 mmol). The mixture was stirred for 1 h. Evaporation of the solvent in vacuo gave an oil which was

stirred with Et$_2$O (30 cm$^3$) to afford **2c** as purple microcrystals. Yield, 0.29 g, 78%. Anal. Found: C, 47.44; H, 7.01. C$_{28}$H$_{48}$ClMnO$_7$P$_2$S$_2$ requires C, 47.16; H, 6.78%. IR (CH$_2$Cl$_2$, cm$^{-1}$) $\nu$(CO): 2030 vs, 1963 s, 1940 s. $^1$H NMR $\delta$ 2.92 (m, 3H, C$H$ of Cy), 2.02–1.15 (m, 45H, C$H_2$ of Et and Cy, and C$H_3$ of Et). $^{31}$P{$^1$H} NMR $\delta$ 44.7 (s (broad), Mn$P$Et$_3$), 29.1 (d, $J$(PP) = 10 Hz, S$_2$C$P$Cy$_3$).

### 3.2. cis,trans-[Mn(CO)$_2$(PEt$_3$)$_2$(S$_2$CPCy$_3$)]ClO$_4$ (3b)

A mixture of $mer,trans$-[Mn(CO)$_3$(PEt$_3$)$_2$Br] [2] (0.273 g, 0.6 mmol) and AgClO$_4$ (0.25 g, 1.2 mmol) in CH$_2$Cl$_2$ (25 cm$^3$) was stirred in the dark for 4 h and then filtered to obtain a yellow solution of $mer,trans$-[Mn(CO)$_3$(PEt$_3$)$_2$(OClO$_3$)]($\nu$(CO) bands at 2040 w, 1950 s, and 1905 s, cm$^{-1}$) [2]. To this was added S$_2$CPCy$_3$ (0.214 g, 0.6 mmol), and CS$_2$ (2 cm$^3$). The mixture was irradiated with UV light for 20 min. The colour changed from red to deep blue. Evaporation of the solvent in vacuo, followed by addition of Et$_2$O (20 cm$^3$) gave **3b** as a deep blue microcrystalline solid. Yield, 0.323 g, 67%. Anal Found: C, 49.67; H, 8.05. C$_{33}$H$_{63}$ClMnO$_6$P$_3$S$_2$ requires C, 49.34; H, 7.91%. IR (CH$_2$Cl$_2$, cm$^{-1}$)$\nu$(CO): 1937 s, 1873 s. $^1$H NMR $\delta$ 2.87 (m, 3H, C$H$ of Cy), 2.05–1.23 (m, 60 H, C$H_2$ of Et and Cy, and C$H_3$ of Et). $^{31}$P{$^1$H} NMR $\delta$ 54.0 (s (broad), Mn$P$Et$_3$), 19.2 (t,$J$(PP) = 13 Hz, S$_2$C$P$Cy$_3$).

### 3.3. Reduction of 3c with sodium amalgam

A solution of **3c** (0.32 g, 0.51 mmol) in THF (20 cm$^3$) was stirred with an excess of 1% Na[Hg] (2 g) at room temperature. The colour changed slowly from deep blue to purple, and then to red. The IR spectra in solutions showed bands at 1883 s, and 1833 m, cm$^{-1}$, together with those of the starting **3c** (1937 s, 1873 s, cm$^{-1}$), and the neutral dithioformate complex $cis,trans$-[Mn(CO)$_2$(PEt$_3$)$_2$(S$_2$CH)] (7, 1926 s, 1856 s, cm$^{-1}$). The solution was transferred over solid [4-CH$_3$–C$_6$H$_4$–N$_2$]PF$_6$ (0.27 g, 1.02 mmol), and the mixture stirred for 15 min and then filtered. The filtrate was evaporated in vacuo, and the residue extracted with hexane (3 × 20 ml) to give a red solution. Evaporation of the solvent gave **7** as red microcrystals. Yield, 0.12 g, 29%. The oily, blue residue (0.04 g) consists mainly of starting **3c**, according to its IR spectrum.

### 3.4. Structure determination of (1)

Crystals suitable for an X-ray determination were grown by slow diffusion of hexane into concentrated solutions of the compound in CH$_2$Cl$_2$. Selected crystallographic details are given in Table 3. Unit cell parameters were determined from the least squares refinement of a set of 25 centred reflections. Three reflections were

measured every hour as orientation and intensity control. Significant decay was not observed. An empirical (psi-scan) absorption correction was applied. Heavy atoms were located from a Patterson synthesis, and the remaining non-hydrogen atoms by DIRDIF [8]. Full-matrix least squares refinements were made with SHELX76 [9]. The drawing on Fig. 2 was made with PLATON (EUCLID Package) [10]. The full list of atomic parameters for hydrogen atoms, and anisotropic thermal parameters for non-hydrogen atoms is available from the Cambridge Crystallographic Data Centre.

### 3.5. Computational details for the MO calculations

Calculations were carried out at the extended Hückel level [11], on the model compounds **1b**, **2d**, and **3d**, by the weighted $H_{ij}$ formula [12]. Standard atomic parameters were taken for H, C, O, S, and P, while those for Mn were taken from the literature [13].

In our structural model the hydrogen atoms replace the terminal groups in the phosphine ligands. In all calculations we used the following bond distances: Mn–P = 2.305, Mn–C = 1.784, Mn–S = 2.364, C–O = 1.156, S–C = 1.700, C–P = 1.795, and P–H = 1.437 Å. The angles around the manganese atoms were idealized to 90°, except for S–Mn–S = 72.8°. All calculations were made at the University of Oviedo on the Scientific Computer Center and X-ray group VAX-computers, with a locally modified version of the program ICON.

### Acknowledgement

### References

[1] D. Miguel, V. Riera, J.A. Miguel, C. Bois, M. Philoche-Levi-salles and Y. Jeannin, J. Chem. Soc. Dalton Trans., (1987) 2875.

[2] D. Miguel, V. Riera, J.A. Miguel, F. Diego, C. Bois and Y. Jeannin, J. Chem. Soc. Dalton Trans., (1990) 2719.

[3] D. Miguel, V. Riera and J.A. Miguel, J. Organomet. Chem., 412 (1991) 127.

[4] N.C. Brown, G.A. Carriedo, N.G. Connelly, F.J. García-Alonso, I.C. Quarmby, A.L. Rieger, P.H. Rieger, V. Riera and M. Vivanco, J. Chem. Soc. Dalton Trans., (1994) 3745; see also G. Pacchioni, and P.S. Bagus, Inorg. Chem., 31 (1992) 4391.

[5] F.L. Wimmer, M.R. Snow and A.M. Bond, Inorg. Chem., 13 (1974) 1617.

[6] B.E. Bursten, J. Am. Chem. Soc., 104 (1982) 1299.

[7] B.E. Bursten, D.J. Darensbourg, G.E. Kellog and D.L. Lichtenberger, Inorg. Chem., 23 (1984) 4361.

[8] P.T. Beurskens, G. Admiraal, W.P. Bosman, G. Beurskens, H.M. Doesburg, S. García-Granda, R.O. Gould, J.M.M. Smits and C. Smikalla, The DIRDIF Program System, Technical Report of the Crystallography Laboratory, 1982 (University of Nijmegen, Netherlands).

[9] G.M. Sheldrick, SHELX76, Program for Crystal Structure Determinations, 1976 (University of Cambridge). Local Version: F.J. van der Maelen, Ph. D. Thesis, University of Oviedo, Oviedo, Spain, 1991.

[10] A.L. Spek, The EUCLID package, in E. Sayre (ed.), Computational Crystallography; Clarendon, Oxford, 1982, p. 528.

[11] R. Hoffmann, J. Chem. Phys., 39 (1963) 1397.

[12] J.H. Ammeter, H.-B. Bürgi, J. Thibault and R. Hoffmann, J. Am. Chem. Soc., 100 (1978) 3686.

[13] M. Elian and R. Hoffmann, Inorg. Chem., 14 (1975) 1058.